DLANN-CA MODELLER FOR FUTURE CROPLAND CHANGE DETECTION USING SATELLITE TIME-SERIES IMAGERY: A CASE STUDY OF VIJAYAWADA, AP, INDIA

Abstract

For applications, say sustainable crop monitoring, food security, along with land and agriculture planning as well as management, it is imperative to detect future changes in CropLand Areas (CLA). This paper aims to precisely envisage future changes in CLA of Vijayawada city of Andhra Pradesh, India, for maintaining the present CLA as well as control future CropLand (CL) deprivation. Thus, to attain this objective, here, future CL change is detected on the base of Deep Learning Artificial Neural Network and Cellular Automata (DLANN-CA) system utilizing Satellites Time-Series Imagery (STSI). Initially, the Satellite Images (SI) of Vijayawada in the year of 1999, 2009, and 2019 are gathered and pre-processed to ameliorate the images' quality. Pre-processing the image will eradicate the distortion, say Geometric Distortions (GD), Cloud and Cloud Shadow (CCS), and atmospheric distortions; and then, utilizing Gaussian based Median Filter (GaMF), the Speckle Noise (SN) as of the SI are filtered effectively. After that, AdamNC based Multi-Level Thresholding (AdamNC-MT) segmentation is employed to segment CLA as of the satellite maps for a CL change prediction. The DLANN-CA was trained centered on these images to produce future maps of 2030 and 2040. Next, centered on the resulting maps, the CL changes between 1999 and 2040 are analyzed. At last, numerical simulation outcomes are rendered to exhibit the proposed method's effectiveness.

Authors

Satyanaraya Reddy Beeram
Associate Professor
KKR & KSR Institute of Technology and Sciences
Guntur, AP, India.

Neela Sundari Pothuri
Assistant Professor
KKR & KSR Institute of Technology and Sciences
Guntur, AP, India.

Vijaya Lakshmi Sannapureddy
Assistant Professor
KKR & KSR Institute of Technology and Sciences
Guntur, AP, India.

M.V.Sheela Devi
Assistant Professor
KKR & KSR Institute of Technology and Sciences
Guntur, AP, India.

Keywords: Satellite Time-Series Imagery, Cropland area, Gaussian based Median Filter (GaMF), AdamNC based Multi-Level Threshoding (AdamNC-MT), Deep Learning Artificial Neural Network and Cellular Automata (DLANN-CA).

I. INTRODUCTION

Several developing economies rely on CL since it contributes direct employment, Gross Domestic Products (GDP), export earnings, raw materials along with food security for disparate sectors [1]. It is anticipated that the world populace will augment from 7.3 billion to 8.7 billion by 2030, 9.7 billion by 2040, and also 11.2 billion by 2100 [2]. And also it is predicted that this population growth outnumbers its ability to generate adequate food to meet demand particularly rice in addition to wheat that is the '2' major staple crops [3]. In this current century, numerous rigorous droughts damaged the national as well as regional crop production drastically. Individual case studies that were done so far have revealed that over the past '3' decades, there was a loss of CL globally (for instance, China, Turkey, the United States, Egypt, together with India). Over 60 percent of the earth's irrigated CL is present close to urban regions [4]. Mostly, the CL loss is due to urban development [5], which is because, in the majority of the globe, unexpected development of cities has brought about a reduction in vegetated regions, wetlands, and also other natural habitats harboring biodiversity [6].

Agricultural expansion along with intensification is projected to augment with global crop demand of food, livestock feed, along with biofuels that are estimated to double by 2040 [7]. The CL expansion is mostly connected to deforestation along with biodiversity loss, chiefly for sensitive ecosystems [8]. Thus, monitoring as well as estimating the CL change patterns over the regions is quite essential to fulfill the obligation for augmenting the populace demand [9]. Comprehending the spatial in addition to temporal dynamics of CL is vital for regular scrutinizing of agricultural yield, supporting the administration of land and water resources, or tracing and comprehending the agriculture's environmental effects [10]. Effectively as well as accurately detecting the present and future CLA is a requisite for accurate agriculture, say phenology detection, crop condition monitoring, yield forecast, and disaster diminution, and is of utmost significance aimed at macroeconomics, food security, agricultural policy-making in addition to environmental protection [11]. For analyzing CL change and developing plans for the proper administration of CL, a larger quantity of information is needed [12].

Satellite Remote Sensing (RS) is an exclusive data source for CL detection over larger areas [13]. For more than '3' decades, an assortment of techniques of RS has been commenced to ascertain plant conditions together with vegetation characteristics [14]. Nevertheless, Time-Series (TS) analysis was extensively employed to map CL in addition to CL information. TS-mapping techniques detect accurately analogized to single-date mapping techniques [15]. It maps as well as predicts Land Use Land Cover (LULC) changes, particularly in the crop rotation of agriculture, deforestation evaluation, yield appraisal, and yield assessment, coastal zone changes, land deprivation detection, vegetation mapping, wetland landscape changes, urban Change Detection (CD), together with other applications [16].

Support Vector Machines (SVM) [17], decision tree algorithms, clustering algorithms, Fourier harmonic analysis, Randoms Forest (RF), spectral matching techniques, number of machine learning, together with Deep Learning (DL) algorithms [18] are some methods and techniques that are taken for crop change prediction. Amongst these, the DL could automatically study internal feature depictions with multiple levels as of original images as

an alternative to the empirical feature design and has verified to be extremely effective in image classification along with object detection [19]. Thus, this paper proposes a future CL CD utilizing RS-TS imagery centered on DL to attain a good environment development.

The paper is pre-arranged as: Section 2 illustrates associated works with a concise summary of the contributions presented in the past. In Section 3, the proposed methodology is explained in a detailed manner with suitable schematic representations. Section 4 elucidates the experimental outcomes, followed by the conclusion in Section 5.

II. RELATED WORKS

Jiage Chen et al. [20] propounded a phonological trajectory (PJ) similarity approach. This approach explored the alterations betwixt 2 TS images. A PJ was built utilizing a multi-harmonic framework to get intra-annual alterations on account of the multiplex spectral–temporal traits of CL. Subsequently, PJ similarity was gauged utilizing coefficient vector differences, and utilized for discovering no-change/change regions. At last, the distance betwixt the type of reference change and the coefficient ratio vectors of the change-pixels were evaluated to discover the exactly altered types.

Lan H. Nguyen et al. [21] rendered a complete perspective of CL conversion in South Dakota. For which, a trajectory-centric analysis that regarded the entire satellite-centric LULC-TS was utilized for meliorating the change detection (CD). In this approach, the input map series were initially transmuted into binary TS. As of this binary series, locations were discovered with a robust temporal signal of being "CL" or "non-CL". At last, the alterations that happened in CL during 2007 -2015 were recognized grounded on pixels' values of input maps.

Juliana Useya et al. [22] mapped the CLs utilizing an automated classification framework. The normalized difference vegetation index (NDVI) and bare-soil index thresholding (that is, NDVI-BSI) and multi-classifier scheme (MCS) were utilized and the spatio-temporal CL changes were ascertained. CD was effectuated via a post-classification statistical approach. The outcomes exposed that NDVI-BSI and MCS executed the best and acquired 80.54% and 79.32% - overall accuracies for 2013, and 87.90% and 88.56%-accuracies for 2018, respectively. This approach was robust and could be automated speedily and easily without loading training data.

Zhihui Wang et al. [23] proffered an approach for a continual CD for 2 sorts of LULC like CL and grassland/mosaic forest, utilizing all existent Landsat data. The vegetation cover-period was primarily recognized utilizing (NDVI) TS. The TS of intra-annual NDVIs was then built at a one-day resolution centered on SG-filtering and linear interpolation. The alteration in Vegetation type was recognized by analogizing the NDVI and NDVI of intra-annual composites. At last, its time of alteration and classification were ascertained with the utilization of decision tree rules built with the integrated- inter- as well as intra-annual NDVI temporal metrics.

Yidi Xua et al. [24] proffered a framework of updating annual CL mapping utilizing a post-classification and CD approaches for meliorating the conventional bi-temporal change vector analyses. The Landsat footprints/regions in Africa (South Africa, Egypt, and Ethiopia) were picked as study areas centered on their disparate field sizes and cropping structures. The

annual changed- regions were recognized by deploying countless thresholds and indices in reference and longer-term annual composite Landsat imageries. Subsequently, the map was updated in the change-pixels utilizing RF-centric classification. The longer-term CL mapping accuracies for these 3 sites were 56.5% to 67.5% for South Africa, 88.04% to 94.3% for Egypt, and 76.2% to 82.8% for Ethiopia.

V. Kumar and S. Agrawal [25] utilized the RS and GIS for detecting the alterations in the agriculture land and its transmutation onto certain LULC types. It recognized the agricultural LULC changes over 18 years (2000-2018). It rendered the data of shrinkage and expansion of open and agriculture land in tehsil extent. Primarily, the Landsat images during 2000-2018 were preprocessed and classified utilizing the Gaussian maximal likelihood. Certain training instances were gathered utilizing ground truth information. Afterward, recognition of LULC changes was made on a pixel-to-pixel basis.

III. FUTURE CROPLAND CHANGE DETECTION USING SATELLITE TIME-SERIES IMAGERY

With respect to global challenges, say population growth, augmenting food demand, along with climate change, the monitoring of CLA encompasses great importance. CLA is quickly changing over time globally because of the climate variability, rural migration to urban regions, industrialization, populace growth, together with other socio-economic issues. In order to attain tenable development, the change of the present CLA can well be effortlessly maintained via monitoring the future forecast of CL images. Here, a future CL change in Vijayawada is predicted centered on DLANN-CA utilizing STSI. The proposed work encompasses ‘3’ phases: i) Preprocessing, ii) Segmentation, and iii) CLA-CD. Initially, the SI from 1999, 2009, and 2019 are gathered, which can present the crucial information of spatial coverage as well as spectral responses of CL for tenable agricultural management. After that, the gathered images are preprocessed for ameliorating the images’ quality. In the preprocessing step, the GD, CCS, and atmospheric distortion are eradicated as of the SI. In addition, the GaMF is utilized to eliminate the SN. Subsequent to preprocessing, the AdamNC-MT is utilized to segment the CLA from the preprocessed images. Subsequently, utilizing the segmented map 1999, 2009, and 2019, the CL image in 2030 and 2040 are predicted utilizing DLANN-CA. At last, centered on the resulting images, the CL changes from 1999 to 2040 are detected. The proposed future CL change detection system’s Workflow is evinced in figure 1.

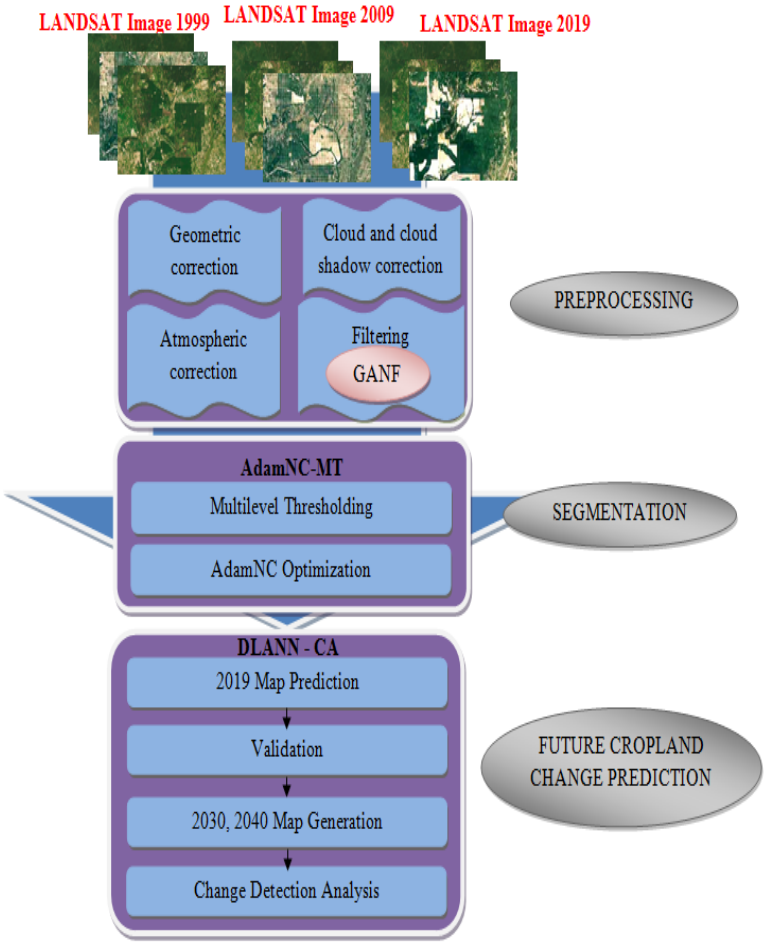

Figure 1: Workflow of Proposed Methodology

1. **Study Area and Satellite Data Acquisition:** Vijayawada is the capital of the Andhra Pradesh, which is the southeast Indian state. It lies on the banks of River Krishna surrounded by the hills of Eastern Ghats with latitude 160311 N and longitude 800 391 E. There are loads of scope for urban development; consequently, there will be rigorous changes on the CLA. Thus, it is vital to envisage the future changes of CL in Vijayawada.

   In google, there are numerous high-qualities STSI, which can well be accessed publically. Thus, SI for the years 1999, 2009, and 2019 are gathered aimed at accurate future CL-CD. These '3' years are chosen, since a longer period (i.e. 10 years) is considered more consistent in capturing the CL changes. Disparate SI has disparate band combinations. Information associated with the CL is acknowledged in the band combination of 4-3-2 (red, green, blue) and 6-5-2 (SWIR-1, near-infrared, blue). Thus, the proposed work utilizes the band combination of (4, 3, 2), and (6, 5, 2).

2. **Preprocessing:** The gathered STSI encompasses disparate sorts of distortion together with noises. Here, preprocessing lessens the reluctant distortions as of the SI and ameliorates the information concerning the crops. Image preprocessing is performed by

subsequent steps: a) Geometric Correction, b) CCS Correction, c) Atmospheric Correction, and d) Noise Filtering.

- **Geometric Correction:** For pre-processing the satellite imagery data as well as eradicating the GD as of a distorted image, this step is vital. Here, initially, the system correction is taken to shun any big systematic distortions. Next, utilizing resampling in addition to interpolation, the image data are changed into a geo-coded image.

- **Cloud and Cloud Shadow Correction:** The CCS as of the SI was eradicated since the pixels without CCS ameliorate the prediction process. The elimination is done on the basis of top-of-atmosphere radiance

- **Atmospheric Correction:** The main aim of this step is to recuperate surface reflectance as of RS-SI via eliminating atmospheric effects. The SI is inputted into the FLAASH (Fast Lines-of-sight Atmospherics Analysis of Spectral Hyper-cubes) to compute surface reflectance intended for images and resolve the atmospherics disturbance issues.

- **Filtering using GaMF:** The Geometric, atmospheric along with CCS corrected images will encompass SN that will demean the image's quality as well as restrict the utilization of CD centered upon statistical assumptions. Therefore, noise filtering is essential prior to utilizing the TS data for additional analyses. Gaussian Median Filtering (GaMF) is employed to filter the SN as of the SI. Though the conventional Median Filter (MF) eliminates the SN completely, its edge-preserving criteria are bad. The gaussian Edge Stopping function (ESF) is employed in the MF technique for eliminating the blurriness and attaining edge preservation. The input image with SN is mathematically signified as,

$$\mathcal{S}(i,j) = S(i,j) * N_s(i,j) \tag{1}$$

Wherein, $\mathcal{S}(i,j)$ implies input noisy image, $S(i,j)$ signifies the original image $N_s(i,j)$ implies the SN in addition to (i,j) signifies the pixel location. The MF is implemented on the chosen bands (4, 3, 2) and (6,5,2) autonomously, and it distinguishes isolated noise that is out-of-range as of original image features, say edges, and lines. Particularly, the MF swaps a pixel by the median (in lieu of the average) of the entire pixels in a neighborhood ξ.

$$M_F(i,j) = med\{\mathcal{S}(i,j),[i,j] \in \xi\} \tag{2}$$

Wherein, $M_F(i,j)$ implies the MF output, ξ signifies a neighbourhood as well as $med\{\bullet\}$ signifies median that is gauged via sorting the entire pixel values as of the adjacent neighborhood into numerical sort, and swapping the pixel being regarded to the mid pixel value. Next, the MF output is implemented to the Gaussian ESF for rendering edge preserved filtered image.

$$M_F''(i,j) \approx M_F(i)_t + \frac{\beta}{|\omega_i|} \sum_{j \in \omega_i} \aleph\left(\nabla\left(\mathcal{G}_\phi * M_F(i,j)_t\right)\right) \tag{3}$$

Wherein, $M_F(i)_t$ implies the i^{th} pixel intensity at instant t, β signifies a scalar associated with the diffusion rate, ω_i implies a compilation of adjacent pixels of i, $\aleph(\bullet)$ implies the ESF, $M_F(i,j)_t$ implies the MF output at instant t, $\mathcal{G}_\phi$ signifies the Gaussian filter of scale ϕ and $M''_F(i,j)$ implies the filtered image. At last, the image (preprocessed) is provided to the next phase, i.e. segmentation, for CL segmentation.

3. **Cropland Segmentation:** AdamNC-MT is employed for segmenting CLA as of the SI of the years 1999, 2009, and 2019. MT is considered as the most basic but dominant technique in segmentation as it partitions an image via selecting disparate Threshold Value (TV), and these TVs are generated arbitrarily. These arbitrary TVs affect the segmentation's effectiveness. Thus, in order to trounce this issue, the proposed technique utilizes AdamNC Optimizer to choose the optimal TV.

In the AG-MT segmentation technique, the intensity of the input preprocessed image $M''_F(i,j)$ at the gray level y is expressed as,

$$I''_F = \{I''_{F1}, I''_{F2,} I''_{F3}, \ldots\ldots, I''_{F\,y-1}\} \tag{4}$$

Here, I''_F implies the preprocessed image's intensity. The gray scale range $\{0,1,\ldots\ldots,y-1\}$ is split into k-number of classes via k-number of threshold values $\hat{t}_k = \{\hat{t}_1, \hat{t}_2, \ldots\ldots \hat{t}_n\}$. The $\hat{t}_k$ was arbitrarily generated. The optimal-TV is attained utilizing AdamNC optimizer. AdamNC is one amongst the Adam optimizer that can render good convergence rates to attain optimal TV. In the AdamNC, the gradient for the inputted TV is calculated.

$$g_{iter} = \nabla f_k(\hat{t}_k)_{iter} \tag{5}$$

Here, $\nabla f_k(\bullet)$ implies the gradient function and $\hat{t}_k$ signifies the inputted-TV at iteration $iter$. Next, the gradient moment estimate is calculated as,

$$A_i = \varpi_{1,iter} A_{iter-1} + (1-\varpi_{1,iter}) g_{iter} \tag{6}$$

$$B_{iter} = \varpi_{2,iter} B_{iter-1} + (1-\varpi_{2,iter}) g^2{}_{iter} \tag{7}$$

Here, A_{iter} and B_{iter} imply the estimates of the 1st moment (the mean) as well as the 2nd moment (the uncentered variance) of the gradients at iteration $iter$ correspondingly, ϖ_1 and ϖ_2 signify decay rates (explicitly, ϖ_1 and ϖ_2 near to 1). AdamNC renders a good convergence rate by augmenting ϖ_1 and lessening ϖ_2. At last, the AdamNC optimizer produces the optimal TV utilizing Eqn. (8).

$$\hat{t}_k{}^* = (\hat{t}_k)_{iter} - \frac{\gamma}{\sqrt{B_{iter}}} A_{iter} \tag{8}$$

$$\overset{\cup}{B}_{iter} = \max(B_{iter-1}, B_{iter}) \tag{9}$$

Here, $\hat{t}_k^{\,*}$ signifies the optimal TV, γ implies learning rate and $\overset{\cup}{B}_{iter}$ signifies the improved B_{iter}. In lieu of utilizing B_{iter} directly, the previous B_{iter-1} is employed, if it outweighs the present one. The optimal TV is expressed as $\hat{t}_k^{\,*} = \{\hat{t}_1^{\,*}, \hat{t}_2^{\,*}, \ldots . \hat{t}_n^{\,*}\}$. Subsequent to attaining the optimal TV, the gray-scale probability occurrence, explicitly, histogram of image $M_F''(i, j)$ is ρ_k'' that is calculated as,

$$\rho_k'' = \frac{X_k}{x} \tag{10}$$

Wherein, X_k implies the number of pixels having gray-level and x signifies the total pixels on a provided image. The probability along with the mean target of every class is calculated as,

$$\alpha_0(\hat{t}_k^{\,*}) = \sum_{k=0}^{\hat{t}_1 - 1} \rho_k'' \qquad \beta_0(\hat{t}_k^{\,*}) = \sum_{k=0}^{\hat{t}_1^{\,*} - 1} \frac{k\rho_k''}{\alpha_0} \tag{11}$$

$$\alpha_1(\hat{t}_k^{\,*}) = \sum_{k=\hat{t}_1^{\,*}}^{\hat{t}_2^{\,*} - 1} \rho_k'' \qquad \beta_1(\hat{t}_k^{\,*}) = \sum_{k=\hat{t}_1^{\,*}}^{\hat{t}_2^{\,*} - 1} \frac{k\rho_k''}{\alpha_1}$$

M (12)

$$\alpha_{k-1}(\hat{t}_k^{\,*}) = \sum_{k=\hat{t}_{k-1}^{\,*}+1}^{\hat{t}_k} \rho_k'' \qquad \beta_{k-1}(\hat{t}_k^{\,*}) = \sum_{k=\hat{t}_{k-1}^{\,*}+1}^{\hat{t}_k^{\,*}} \frac{k\rho_k''}{\alpha_{k-1}}$$

$$\alpha_k(\hat{t}_k^{\,*}) = \sum_{k=\hat{t}_k^{\,*}}^{y-1} \rho_k'' \qquad \beta_k(\hat{t}_k^{\,*}) = \sum_{k=\hat{t}_k^{\,*}}^{y-1} \frac{k\rho_k''}{\alpha_k} \tag{13}$$

Centered on these probabilities in addition to mean target value, the between-class variance of k-number of class can be attained as,

$$\begin{aligned} Q(\hat{t}_1^{\,*}, \hat{t}_2^{\,*}, \ldots . \hat{t}_k^{\,*}) = {} & \alpha_0\alpha_1(\beta_0 - \beta_1)^2 + \alpha_0\alpha_2(\beta_0 - \beta_2)^2 + \ldots . + \alpha_0\alpha_k(\beta_0 - \beta_k)^2 + \\ & \alpha_1\alpha_2(\beta_1 - \beta_2)^2 + \alpha_1\alpha_2(\beta_1 - \beta_2)^2 + \ldots . + \alpha_{k-1}\alpha_k(\beta_{k-1} - \beta_k)^2 \end{aligned} \tag{14}$$

Centered on $Q(\hat{t}_1^{\,*}, \hat{t}_2^{\,*}, \ldots . \hat{t}_k^{\,*})$ along with image pixel value I_F'', the CLA as of the SI was segmented. If $I_F'' > Q(\hat{t}_1^{\,*}, \hat{t}_2^{\,*}, \ldots . \hat{t}_k^{\,*})$, set a pixel value in the image as white (1) or else set a pixel value on the image as black (0). The resulting image has just '2' regions: black and white. This way, every pixel as per CLA was segmented as of the SI in the year

of 1999, 2009, and 2019 utilizing the ANC-MT method. The resulting CL map images of 1999, 2009, and 2019 are examined and the future CD was performed. The AdamNC-MT pseudocode is evinced in figure 2.

Input: Satellite Images of 1999, 2009 and 2019
Output: Segmented Cropland Image of 1999, 2009 and 2019

Begin
Initialize intensity of preprocessed image $M''_F(i,j)$
Generate k-number of threshold values $\hat{t}_k = \{\hat{t}_1, \hat{t}_2, ..., \hat{t}_n\}$
for $\hat{t}_1 = 0$ to $\hat{t}_k$ **do**
{
Set $A_{iter} = 0$, $B_{iter} = 0$ and $\vec{B}_{iter} = 0$
for $iter = 0$ to $iter_{max}$ **do**

$$\hat{t}_k^{\,*} = (\hat{t}_k)_{iter} - \frac{\gamma}{\sqrt{\vec{B}_{iter}}} A_{iter} \qquad \text{//Threshold Optimization}$$

end for
}
Calculate occurrence distribution of probability ρ''_k
Divide image pixel into k-number of class
Calculate probability and mean target for each class
Calculate between-class variance $\mathcal{Q}(\hat{t}_1^{\,*}, \hat{t}_2^{\,*}, ..., \hat{t}_k^{\,*})$
if $(I''_F > \mathcal{Q}(\hat{t}_1^{\,*}, \hat{t}_2^{\,*}, ..., \hat{t}_k^{\,*}))$
Set to pixel value in image as white
else if
Set to pixel value in image as black
end if
end for
Return Segmented Images
End

Figure 2: Pseudocode of AdamNC-MT Segmentation

4. **Future Cropland Change Detection:** Area CD analysis is employed to envisage the possible change areas during the full-TS. The output maps of '3' disparate decades attained as of the segmentation process are inputted to the Land Change Modeller (LCM) to carry-out future CL-CD. The proposed work employs a DLANN-CA as an LCM. The ANN is utilized extensively in CD, pattern recognition, along with categorization in a gamut of applications on account of its accuracy, efficiency, together with competence to

model non-linear relations. The DLANN performs the learning procedure intensely through boosting the total Hidden Layers (HL). This DL process lessens the network training error. The DLANN is utilized for ascertaining the transition probability of CL changes utilizing manifold output neurons. Via implementing this transition probability, the CA designs the future CL changes.

The DLANN comprises '3' layers, i) one Input Layer (IL), ii) above one HL, together with iii) one Output Layer (OL), and every layer comprises many neurons. DLANN's structure is evinced in figure 3. Initially, the segmented CL maps (1999 and 2009) are inputted into the DLANN layer meant for producing a CL map for 2019. The simulation is pixel (cell)-centered; every pixel encompasses n-number of spatial variables that are inputted for training the neurons aimed at modelling CL changes. Initially, the inputted values are mapped into the HL. The activation ($\Phi(f)$) function is then generated, which is written as,

$$\Phi(f) = \sum_u \tilde{W}_{uv} I_u^n \tag{15}$$

Wherein, I_u^n implies the u^{th} scaled attribute related to the u^{th} neuron on the IL, $\tilde{W}_{uv}$ implies the weight value between IL and HL. The DLANN adopted the Gaussian activation function. Every neuron on the HL receives the values as of the IL neuron, which is expressed as,

$$O_v^{n+1} = f_\rho\left(\sum_u \tilde{W}_{uv} I_u^n + bias_v\right) \tag{16}$$

Wherein, O_v^{n+1} implies the output of the v^{th} neuron on the HL, $bias_v$ signifies the bias value of the v^{th} neuron on the HL, and $f_\rho(\bullet)$ implies the transition function.

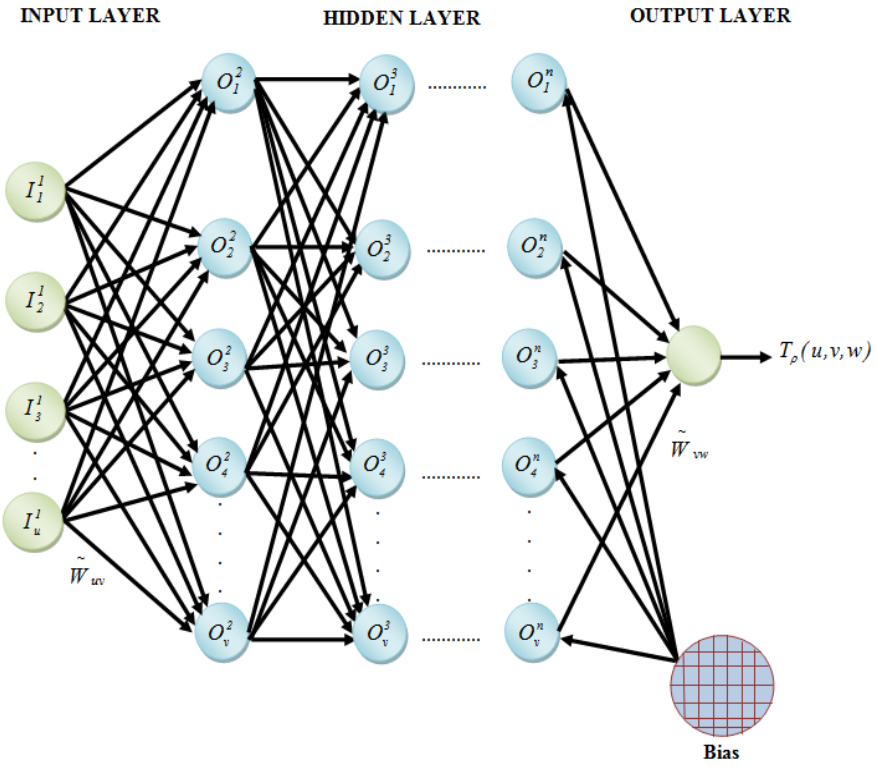

Figure 3: Structure of DLANN

The HL output mapped to the OL and w^{th} neuron in the OL generates the transition probability as of the initial type to the target type of CL. The transition probability is generated as,

$$T_\rho(u,v,w) = \sum_v \tilde{W}_{vw} \frac{1}{1+\exp\left(O_v^{n+1}\right)} \tag{17}$$

Here,

$T_\rho(u,v,w)$ - Transition probability

(u,v,w) - IL, HL, OL, respectively

$\tilde{W}_{vw}$ - Weight value betwixt HL and OL.

During iterations, $T_\rho(u,v,w)$ is created by the OL's neurons. Once it is created, the CA simulation is performed for modeling CL change. CA stands as a bottom-up dynamic approach with a spatio-temporal computation. It is discrete in state and space-time, and it could execute complex time-space simulations. Here, the pre-determined TV is utilized to handle the rate of change in order that land-use conversions transpire step-by-step. If TV $< T_\rho(u,v,w)$, then the pixel remains unaltered. In this manner, the CL map for 2019 was predicted centered on the transition probability of CL segmented images of 1999 and 2009. Then, the predicted land map-2019 is checked out with the actual segmented map of 2019 regarding sensitivity, Negative Prediction Value (NPV), precision, False Positive

Rate (FPR), specificity, False Negative Rate (FNR), accuracy, F-measure, Mathew's Correlation Coefficient (MCC), Kappa Coefficient (KC) together with False Rejection Rates (FRR). The proposed future CL map prediction could be comprehended with the below flowchart (figure 4),

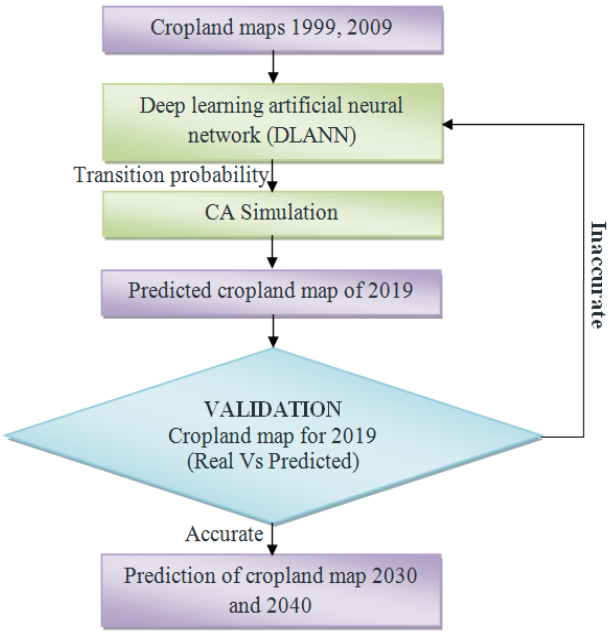

Figure 4: Flowchart of Proposed Future CL Prediction

The validation process is assessed by analogizing the predicted map of 2019 and the real map of 2019 for verifying the proposed CD system's performance. The simulation process is repeated till the acceptable sensitivity, specificity, accuracy, precision, F-measure, NPV, FPR, FNR, MCC, FRR, and KC are acquired. When all the quality metric values are acceptable, the CL in 2030 and 2040 can be predicted utilizing CL map 1999, 2009, and 2019.

Change Detection Analysis: The CD statistical analysis is an effectual way of representing the changes perceived in the CLA. The estimated CLA is derived from the maps of the years 1999 to 2040 using DLANN-CA. The land changes are evaluated as,

$$Land\,Change = \frac{F_{stage} - I_{stage}}{I_{stage}} \times 100 \tag{18}$$

Here,

F_{stage} - CL's final stage

I_{stage} - CL's initial stage

The land change is generally signified in percentage. The knowledge of CLA change is necessary for assessing the present status, planning the future challenges associated to food security, environmental climate change, elevated CO_2 emissions, etc., and ensuring the sustainability of the existent resources.

IV. RESULT AND DISCUSSION

The results of the experiments are analyzed to verify the proposed model's performance for evaluating its effectiveness. The proposed AdamNC-MT and DLANN-CA utilized for segmentation and future CL prediction are contrasted against some existing approaches under certain quality metrics. This work utilizes SIs taken in the1999, 2009, and 2019 decades for performance evaluation, which are gathered as of the publically existent dataset. Here, figure 5 signifies the (a) input images in the years of 1999, 2009, and 2019 (b) Preprocessed images, along with (c) segmented CL images for 1999, 2009, and 2019 years.

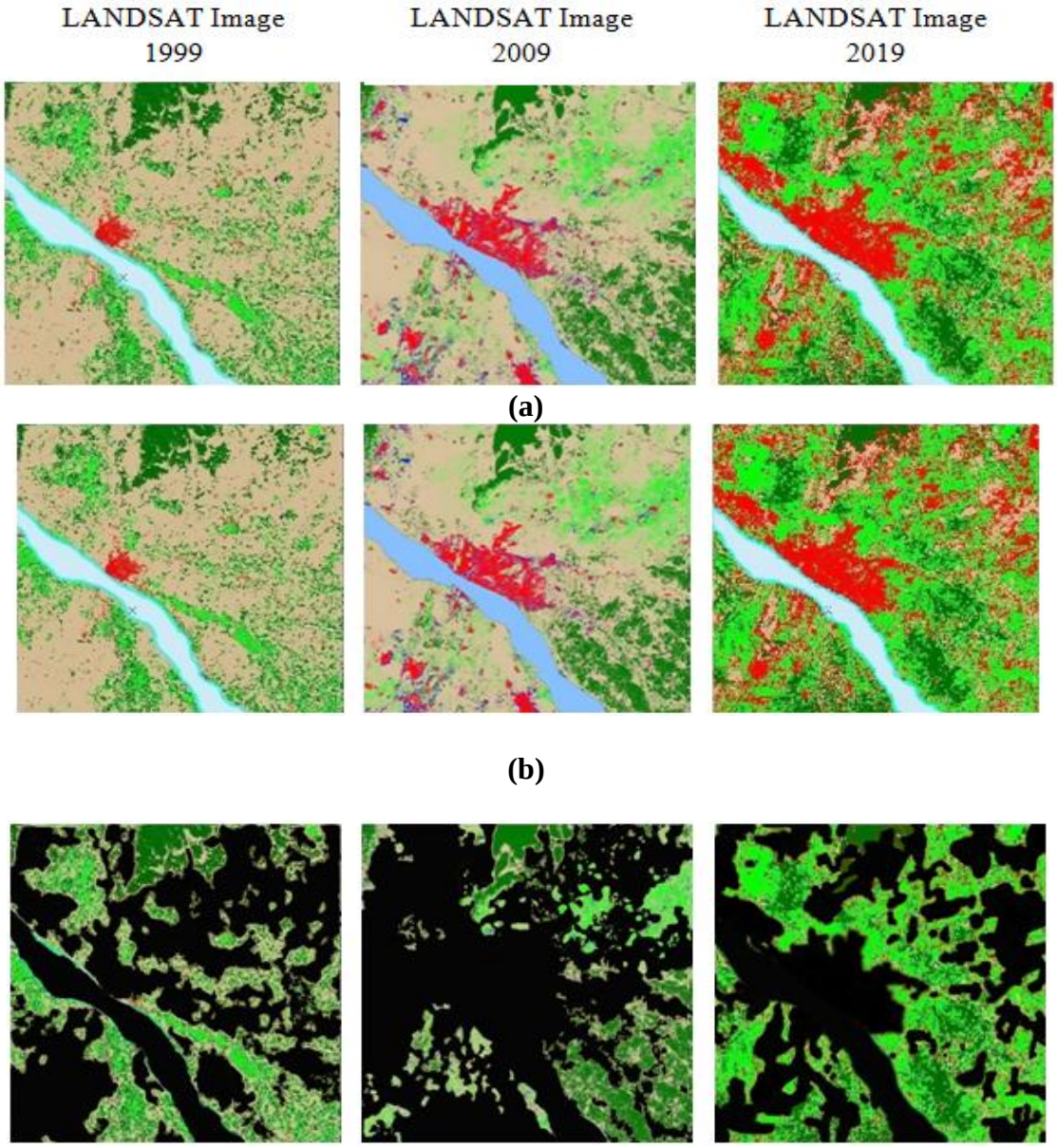

Figure 5: CL map of study area for 1999, 2009 & 2019
(a) Input images (b) Preprocessed images (c) Segmented image of CLs

The 2019 CL map is predicted grounded on CL maps of 1999 and 2009. Likewise, the CL map of 2030 and 2040 could be predicted using1999, 2009 and 2019 CL maps. Figure 6 clearly depicted these predicted maps.

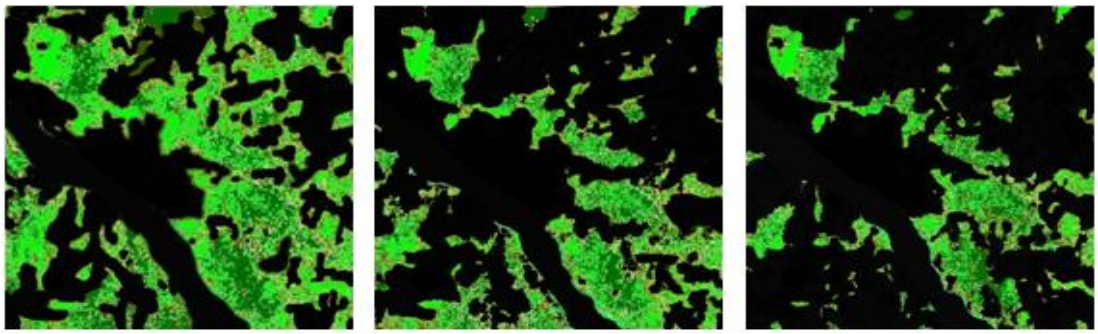

(a) **(b)** **(c)**

Figure 6: Predicted CL maps in the year of (a) 2019 (b) 2030 (c) 2040

The above figures explicate that the CLA of Vijayawada city will significantly decrease between 2019 and 2040. This significant change might be on account of infrastructure development as well as rapid urbanization. Hence, stringent development control regulations have to be framed and executed centered on the future CL prediction results for ensuring orderly and regulated growth of the urbanized regions, thereby directing to the sustainable development of the study area "Vijayawada city".

The performance is analyzed to check the prediction efficiencies of the proposed approaches, which is explicated in the below section.

Performance Analysis of AdamNC-MT Technique: Here, the AdamNC-MT which is proposed as a segmentation methodology for segmenting the CLA as of the preprocessed SI is analyzed by analogizing it with the existing techniques, say Muti-Level Thresholding (MT), Region Growing (RG), Fuzzy C-Means (FCM), and Level Set centered on their performance regarding the rand index (RI), sensitivity, accuracy, variation of information (VI), specificity, along with global consistency error (GCE). The sensitivity, accuracy, RI, specificity, GCE, and VI values acquired by the proposed and existing are evaluated and enumerated using table 1.

Table 1: Segmentation Techniques Performance Comparison

Metrics	Proposed AdamNC-MT	Multi-Level Thresholding	Region growing	Level set	FCM
Accuracy	0.98	0.964	0.97	0.95	0.943
Sensitivity	0.982	0.959	0.973	0.96	0.934
Specificity	0.978	0.952	0.961	0.972	0.92
RI	0.97	0.95	0.957	0.962	0.94

GCE	0.0042	0.018	0.015	0.0072	0.02
VI	0.059	0.25	0.07	0.081	0.32

Table 1 contrasts the proposed and existing segmentation approaches centered on performance in respect of sensitivity, accuracy, RI, specificity, GCE, and VI. For an effective segmentation, the techniques should render high specificity, accuracy, sensitivity, and RI and low GCE and VI. From table-1, the proposed AdamNC-MT outweighs the existing MT, RG, Level set, and FCM regarding all metrics. Table 1 is graphically explicated using the below figures.

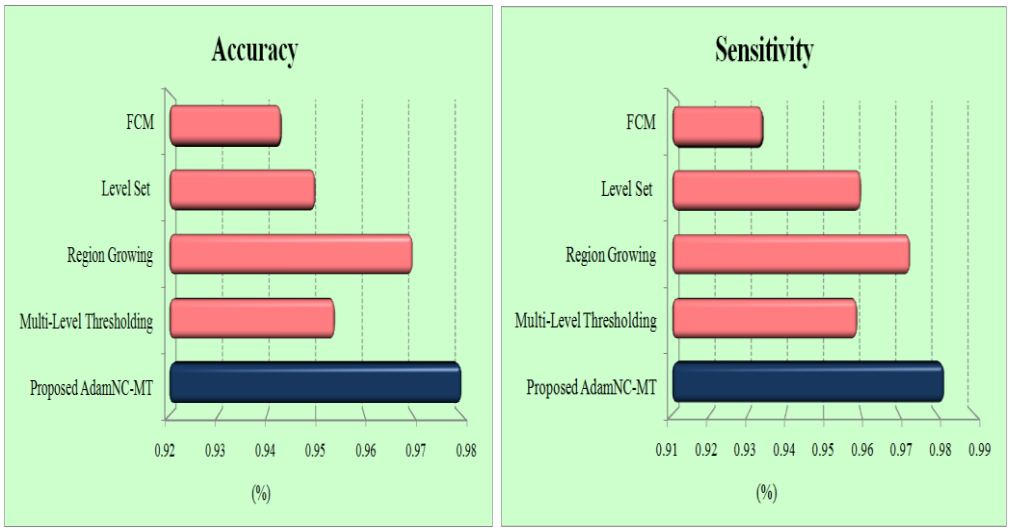

(a) **(b)**

Figure 7: Performance analysis of Proposed and Existing Segmentation Techniques (a) Accuracy (b) Sensitivity

Figure 7(a) contrasts the performance rendered by the proposed and existing segmentation approaches in respect of accuracy. The accuracy metric delineates how accurately the system segments the CL from the SIs. From the figure, the proposed AdamNC-MT shows 0.98-accuracy, whereas the existing MT, RG, Level set, and FCM have 0.964%, 0.97%, 0.95%, and 0.943%- accuracies respectively, which are lower when analogized with the proposed AdamNC-MT. On this account, the proposed AdamNC-MT is found to segment the CLA from the SIs more accurately.

The sensitivity values acquired by the existing and proposed approaches are evaluated utilizing fig 7(b). Sensitivity is the proportion of actual CLA that got segmented as CLA. The existing MT, RG, Level set, and FCM attain 0.959%, 0.97%, 0.95%, and 0.943%, -sensitivities respectively, but the proposed AdamNC-MT acquires 0.982% sensitivity. This comparison shows that the RG method's performance is closer to that of the proposed one. Forbye, the proposed AdamNC-MT shows 0.18%-sensitivity which outweighs the RG technique.

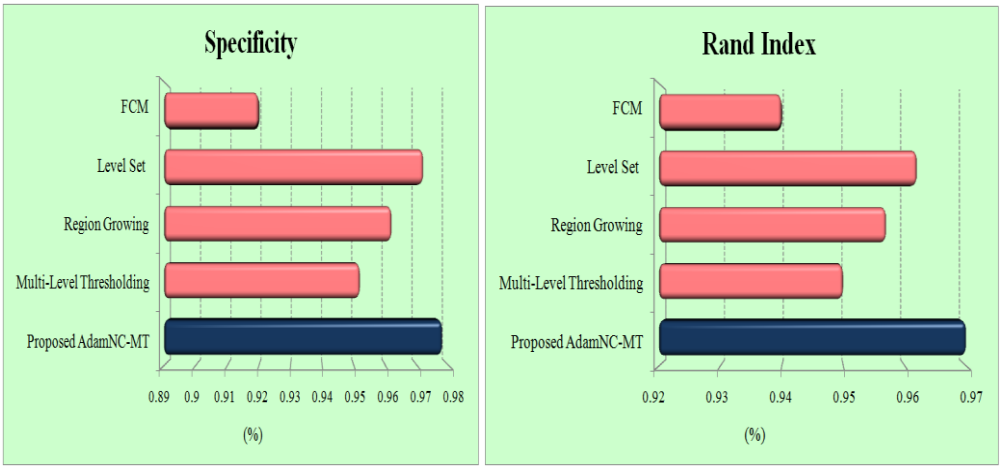

(a) **(b)**

Figure 8: Performance analysis of Proposed and Existing Segmentation Techniques
(a) Specificity (b) Rand Index

Figure 8(a) evinces the performance assessment of disparate segmentation approaches in respect of specificity. Specificity of existing MT, RG, Level set and FCM is 0.952%, 0.961%, 0.972% and 0.92% respectively. But the proposed AdamNC-MT outweighs the existing techniques by showing 0.978%- specificity.

Figure 8(b) analyzes the RI levels of the segmentation techniques. The RI metric gauges the similarity between the original CL and segmented CL. So, for good performance, the system should have high RI. On analyzing figure, proposed AdamNC-MT has RI values of 0.2% higher than MT, 0.13% greater than the RG, 0.08% higher than level set, and 0.3% greater than FCM. From this comparison, the proposed AdamNC-MT is the only approach that proffered the excellent performance.

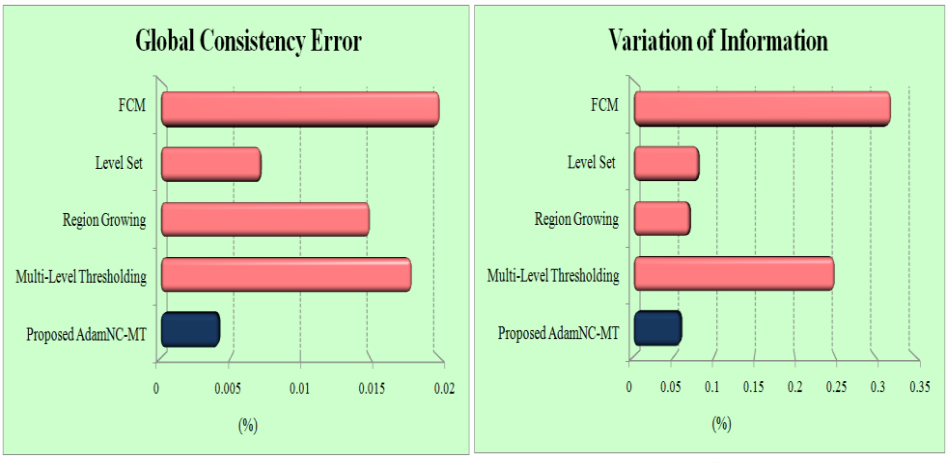

(a) **(b)**

Figure 9: Performance analysis of Proposed and Existing Segmentation Techniques
(a) Global Consistency Error (b) Variation of Information

The proposed AdamNC-MT and existing MT, RG, Level set, and FCM are analogized regarding GCE in fig 9(a). The segmentation approaches should have a lower

GCE for attaining excellent performance. The proposed AdamNC-MT has 0.0042%- GCE level, but the existing RG, Level set and FCM showed 0.018%, 0.015%, 0.0072% and 0.02%. This corroborates that the existing approaches have higher most error values, so their performances are worse as contrasted to the proposed AdamNC-MT.

Figure 9(b) evinces the performance of disparate segmentation approaches in respect of VI. VI gauges the distance between the segmented CL image and the original CL image. On this account, it must be low for effectual segmentation. The proposed AdamNC-MT has only 0.059- VI but all the existing techniques have higher-most VI values.

For all the concerned metrics, the proposed AdamNC-MT algorithm outweighs the existing algorithms. On this account, the proposed AdamNC-MT segmentation algorithm can effectively and accurately segment the CLA than others.

V. PERFORMANCE ANALYSIS OF DLANN-CA TECHNIQUE

This section explicates how effective and accurate the proposed DLANN-CA generates the CL map 2019. The DLANN-CA's effectiveness is checked out by analogizing its performance with the existing ANN, Convolutional Neural Network (CNN), SVM, RF approaches in respect of sensitivity, precision, specificity, NPV, accuracy, F-measure, FPR, FNR, MCC, FRR, and KC.

Table 2: Performance Comparison of Proposed and Existing LCM Techniques based on Statistical Measures

Performance Metrics	Proposed DLANN-CA	Existing ANN	CNN	SVM	RF
Sensitivity	0.97	0.81	0.882	0.881	0.762
Specificity	0.98	0.899	0.944	0.887	0.878
Accuracy	0.99	0.862	0.921	0.872	0.844
Precision	0.959	0.812	0.872	0.815	0.768
F-Measure	0.961	0.822	0.879	0.812	0.762
NPV	0.979	0.91	0.939	0.89	0.882
FPR	0.021	0.13	0.061	0.11	0.126
FNR	0.042	0.25	0.119	0.21	0.242
MCC	0.942	0.72	0.823	0.722	0.648
FRR	0.039	0.21	0.121	0.522	0.244
Kappa Coefficient	0.95	0.82	0.89	0.71	0.86

Table 2 compares the proposed DLANN-CA and existing map prediction modelers say ANN, CNN, SVM, and RF centered on performance regarding 11 statistical metrics. Those metrics are evaluated by analogizing the predicted map of 2019 with the actual map of 2019. For all 11 metrics, the proposed DLANN-CA shows excellent values. So from the performance comparison, the proposed modeler is the only approach that proffered the topmost performance.

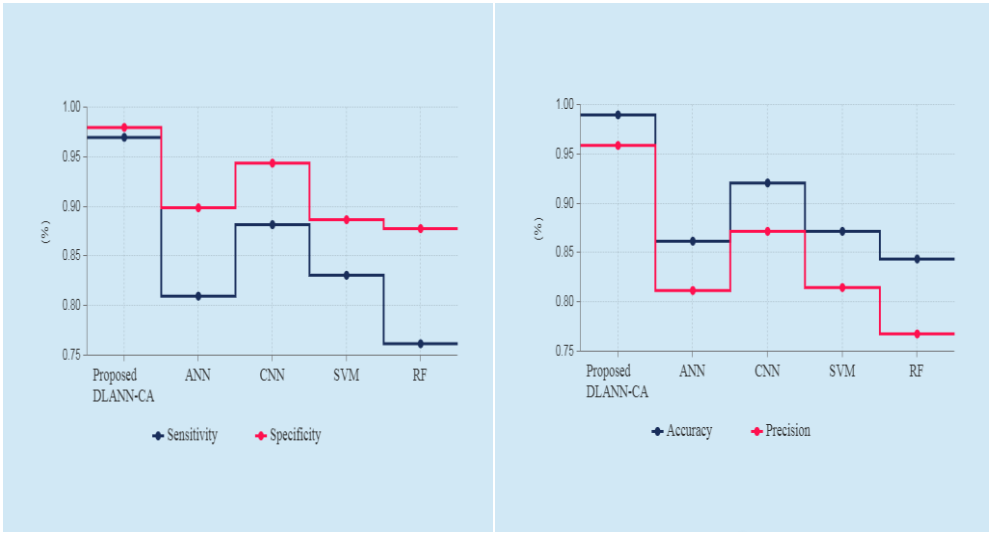

(a) **(b)**

Figure 10: Performance analysis of Proposed and Existing LCM
(a) Sensitivity and Specificity (b) Accuracy and Precision

Figure 10(a) contrasts the performance rendered by the existing and proposed LCM in respect of specificity as well as sensitivity. The sensitivity attained by the existing LCMs like ANN, CNN, SVM, and RF is 0.81%, 0.882%, 0.831%, and 0.76%, respectively, whereas, the proposed DLANN-CA achieves 0.97%. Likewise, the existing ANN, CNN, SVM, and RF showed 0.889%, 0.944%, 0.887%, and 0.878%- specificity values, respectively. But the proposed LCM's specificity is 0.98%, which shows its effectiveness level.

Figure 10(b) evinces the accuracy as well as precision values attained by the proposed and existing LCMs. Accuracy is the notable metric in the land change framework, which delineates how accurately the LCM creates a map. On examining the fig 10(b), the proposed LCM has 0.99- accuracy, which corroborates that it accurately creates the map 2019. The existing LCMs, like ANN, CNN, SVM, and RF create the maps with 0.862%, 0.921%, 0.872%, and 0.844%- accuracies, respectively, which are lesser contrasted to the proposed LCM. In the consideration of precision, the existing ANN, CNN, SVM, and RF attain precision up to 0.821%, 0.872%, 0.815%, and 0.768%, respectively, whereas the proposed DLANN-CA has 0.959%- precision. From these results, the proposed DLANN-CA generated the land maps accurately.

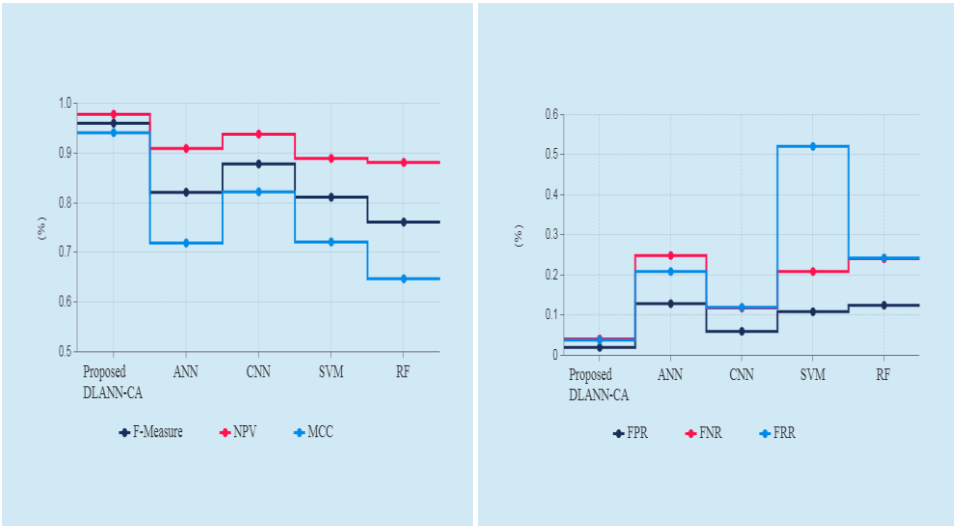

(a) **(b)**

Figure 11: Performance analysis of Proposed and Existing LCM
(a) F-measure, NPV and MCC (b) FPR, FNR and FRR

Figure 11(a) contrasts the performance rendered by the proposed and existing LCM grounded on F-measure, NPV, and MCC. For an accurate map generation system, the system should have a higher F-measure, NPV, and MCC. The proposed DLANN-CA system has 0.961%- F-measure, 0.979%- NPV, and 0.942%- MCC, respectively. After DLANN-CA, CNN proffered a better performance, which has an F-measure, NPV, and MCC of 0.879%, 0.939%, and 0.82%, respectively. Other existing LCMs have lower-most performance compared to CNN and DLANN-CA.

Figure 11(b) analogizes the proposed and existing LCM centered on performance in respect of FPR, FNR, and FRR. Those 3 statistical measures gauge how much error transpired in the system during map prediction. So, FPR, FNR, and FRR should be low for the land change framework. The proposed LCM has 0.021%- FPR, whereas the existing ANN, CNN, SVM, and RF have 0.13%, 0.061%, 0.11%, and 0.126% - FPR values respectively. Contrarily, the proposed DLANN-CA has 0.042%- FNR, and the existing ANN, CNN, SVM, and RF have 0.25%, 0.119%, 0.21%, and 0.242%- FNR values, respectively. Likewise for FRR, the proposed DLANN-CA renders a less FRR when analogized with the existing land change system. From this result, the proposed DLANN-CA outweighs the existing systems regarding FPR, FNR, and FRR.

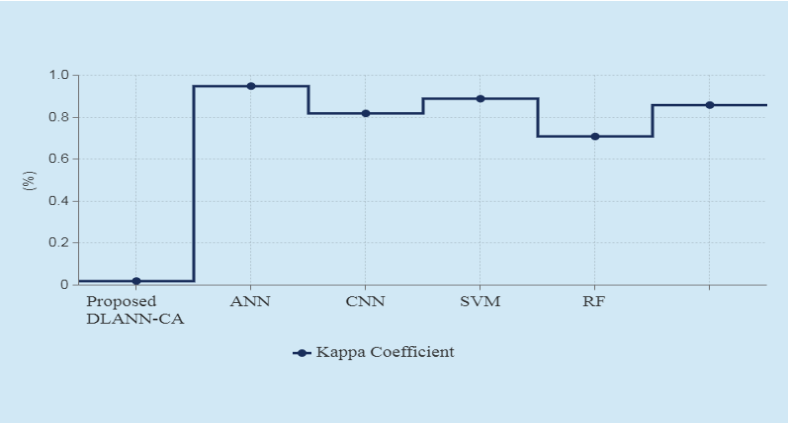

Figure 12: Performance Analysis of Proposed and Existing LCM regarding Kappa Coefficient

Figure 12 signifies the proposed and existing land change system in respect of the KC. The true agreement as of the existing and proposed approaches is gauged by the KC. KC which is an accuracy indicator essentially assesses how well the system performed as contrasted to just arbitrarily allotting values. The KC is evaluated as,

$$\kappa = \frac{\phi_o - \phi_e}{1 - \phi_e} \tag{19}$$

Here,

ϕ_o - Observed agreements proposition,

ϕ_e - Proportion of agreements expected by chance.

The KC ranges as of 0 to 1. If the KC equals 0, then no agreement is found between the reference image and the classified image. If KC is close to 1, then a perfect agreement is found betwixt the real image and the predicted image. The result explicates the agreement of every criterion of every pixel. The proposed system has 0.95- KC, which is closer to 1. The existing ANN, SVM, CNN, and RF have 0.82, 0.71, 0.89, and 0.86, - KC values, respectively. So, the technique that perfectly generated the map is the proposed DLANN-CA. The result comparison corroborates that the proposed work has done a good job in map prediction. Grounded on the 2019 map prediction process, future maps 2030 and 2040 are generated and are almost accurately predicted. This CLA's future prediction is becoming important since most vegetation and CL is being transmuted into the built-up area, which may greatly affect the environment. So, this would assist to maintain the CLA all through the world for acquiring sustainable development.

VI. CONCLUSION

This paper detects the future CL changes of Vijayawada in the year of 2030 and 2040 centered on DLANN-CA using STSI. For this detection, three phases like preprocessing, segmentation, and future CD of CLA, are performed. This work aims to accurately predict future CL changes for maintaining the current CLA. The AdamNC-MT and DLANN-CA are

analogized with some existing approaches centered on performance for verifying their effectiveness. From the attained outcomes, the proposed AdamNC-MT is the only approach that segments the CLA as of the SIs with higher-most accuracy (0.98). Contrarily, the proposed DLANN-CA outweighed the existing ANN, CNN, SVM, and RF in respect of sensitivity, precision, specificity, NPV, accuracy, FPR, F-measure, FNR, KC, MCC, and FRR. The proposed DLANN-CA yielded 0.99- accuracy with 0.95-KC. And also, the DLANN-CA has very low FRR and FNR, which is 0.039 and 0.042. The analysis corroborated that the proposed approaches are more accurate and efficient in future change prediction.

REFERENCES

[1] Juliana Useya, and Shengbo Chen, "Comparative performance evaluation of pixel-level and decision-level data fusion of landsat 8 OLI, landsat 7 ETM+ and sentinel-2 MSI for crop ensemble classification", IEEE Journal of Selected Topics in Applied Earth Observations and Remote Sensing, vol. 11, no. 11, pp. 4441-4451, 2018.

[2] Mariana Belgiu and Ovidiu Csillik, "Sentinel-2 cropland mapping using pixel-based and object-based time-weighted dynamic time warping analysis", Remote sensing of environment, vol. 204, pp. 509-523, 2018, 10.1016/j.rse.2017.10.005.

[3] Murali Krishna Gumma, Prasad S. Thenkabail, Pardhasaradhi G. Teluguntla, Adam Oliphant, Jun Xiong, Chandra Giri, Vineetha Pyla, Sreenath Dixit, and Anthony M. Whitbread, "Agricultural cropland extent and areas of South Asia derived using Landsat satellite 30-m time-series big-data using random forest machine learning algorithms on the Google Earth Engine cloud", GIScience & Remote Sensing, vol. 57, no. 3, pp. 302-322, 2020.

[4] Christopher Bren d'Amour, Femke Reitsma, Giovanni Baiocchi, Stephan Barthel, Burak Güneralp, Karl-Heinz Erb, Helmut Haberl, Felix Creutzig, and Karen C. Seto, "Future urban land expansion and implications for global croplands", Proceedings of the National Academy of Sciences, vol. 114, no. 34, pp. 8939-8944, 2017.

[5] Patrícia Abrantes, Inês Fontes, Eduardo Gomes, and Jorge Rocha, "Compliance of land cover changes with municipal land use planning: Evidence from the Lisbon metropolitan region (1990–2007)", Land Use Policy, vol. 51, pp. 120-134, 2016, 10.1016/j.landusepol.2015.10.023.

[6] Pramit Verma, Aditya Raghubanshi, Prashant K. Srivastava, and A. S. Raghubanshi, "Appraisal of kappa-based metrics and disagreement indices of accuracy assessment for parametric and nonparametric techniques used in LULC classification and change detection", Modeling Earth Systems and Environment, pp. 1-15, 2020, 10.1007/s40808-020-00740-x.

[7] Laura Kehoe, Alfredo Romero-Muñoz, Ester Polaina, Lyndon Estes, Holger Kreft, and Tobias Kuemmerle, "Biodiversity at risk under future cropland expansion and intensification", Nature Ecology & Evolution, vol. 1, no. 8, pp. 1129-1135, 2017.

[8] Katharina Heupel, Daniel Spengler, and Sibylle Itzerott, "A progressive crop-type classification using multitemporal remote sensing data and phenological information", PFG–Journal of Photogrammetry, Remote Sensing and Geoinformation Science, vol. 86, no. 2, pp. 53-69, 2018.

[9] Kabir Uddin, Mir A. Matin, and Franz J. Meyer, "Operational flood mapping using multi-temporal sentinel-1 SAR images: a case study from Bangladesh", Remote Sensing, vol. 11, no. 13, pp. 1581, 2019.

[10] Pengyu Hao, Fabian Löw, and Chandrashekhar Biradar, "Annual cropland mapping using reference landsat time series—A case study in central asia", Remote Sensing, vol. 10, no. 12, pp. 2057, 2018.

[11] Xinkai Liu, Han Zhai, Yonglin Shen, Benke Lou, Changmin Jiang, Tianqi Li, Sayed Bilal Hussain, and Guoling Shen, "Large-scale crop mapping from multisource remote sensing images in google earth engine", IEEE Journal of Selected Topics in Applied Earth Observations and Remote Sensing, vol. 13, pp. 414-427, 2020, 10.1109/JSTARS.2019.2963539.

[12] Xiaobing Zhou, Ni-Bin Chang, and Shusun Li, "Applications of SAR interferometry in earth and environmental science research", Sensors, vol. 9, no. 3, pp. 1876-1912, 2009.

[13] Upadhyay Renu, R. K. Nema, M. K. Awasthi, and Tiwari Y. K, "Change detection analysis of Cropland using Geospatial technique-A case Study of Narsinghpur District", International Journal of Environment, Agriculture and Biotechnology, vol. 2, no. 4, pp. 238845, 2017.

[14] Konrad Hentze, Frank Thonfeld, and Gunter Menz, "Evaluating crop area mapping from MODIS time-series as an assessment tool for Zimbabwe's "fast track land reform programme", PloS one, vol. 11, no. 6, pp. e0156630, 2016.
[15] Vidhee Avashia, Shrutika Parihar, and Amit Garg, "Evaluation of classification techniques for land use change mapping of indian cities", Journal of the Indian Society of Remote Sensing, pp. 1-32, 2020, 10.1007/s12524-020-01122-7.
[16] Yongzheng Ren, Xiao-Ming Li, GuoPing Gao, and Thomas Edmund Busche, "Derivation of sea surface tidal current from spaceborne SAR constellation data", IEEE Transactions on Geoscience and Remote Sensing, vol. 55, no. 6, pp. 3236-3247, 2017.
[17] Maysa Malfiza Garcia de Macedo, Andrea Britto Mattos, and Dário Augusto Borges Oliveira, "Generalization of convolutional LSTM models for crop area estimation", IEEE Journal of Selected Topics in Applied Earth Observations and Remote Sensing, vol. 13, pp. 1134-1142, 2020, 10.1109/JSTARS.2020.2973602.
[18] Jun Xiong, Prasad S. Thenkabail, Murali K. Gumma, Pardhasaradhi Teluguntla, Justin Poehnelt, Russell G. Congalton, Kamini Yadav, and David Thau, "Automated cropland mapping of continental Africa using Google Earth Engine cloud computing", ISPRS Journal of Photogrammetry and Remote Sensing, vol. 126, pp. 225-244, 2017.
[19] Nataliia Kussul, Mykola Lavreniuk, Sergii Skakun, and Andrii Shelestov, "Deep learning classification of land cover and crop types using remote sensing data", IEEE Geoscience and Remote Sensing Letters, vol. 14, no. 5, pp. 778-782, 2017.
[20] Jiage Chen, Jun Chen, Huiping Liu, and Shu Peng, "Detection of cropland change using multi-harmonic based phenological trajectory similarity", Remote Sensing, vol. 10, no. 7, pp. 1020, 2018.
[21] Lan Nguyen H, Deepak R. Joshi, and Geoffrey M. Henebry, "Improved change detection with trajectory-based approach: Application to quantify cropland expansion in South Dakota", Land, vol. 8, no. 4, pp. 57, 2019.
[22] Juliana Useya, Shengbo Chen, and Mike Murefu, "Cropland mapping and change detection: toward zimbabwean cropland inventory", IEEE Access, vol. 7, pp. 53603-53620, 2019, 10.1109/ACCESS.2019.2912807.
[23] Zhihui Wang, Wenyi Yao, Qiuhong Tang, Liangyun Liu, Peiqing Xiao, Xiangbing Kong, Pan Zhang, Fangxin Shi, and Yuanjian Wang, "Continuous change detection of forest/grassland and cropland in the Loess Plateau of China using all available Landsat data", Remote Sensing, vol. 10, no. 11, pp. 1775, 2018.
[24] Yidi Xu, Le Yu, Feng R. Zhao, Xueliang Cai, Jiyao Zhao, Hui Lu, and Peng Gong, "Tracking annual cropland changes from 1984 to 2016 using time-series Landsat images with a change-detection and post-classification approach: Experiments from three sites in Africa", Remote Sensing of Environment, vol. 218, pp. 13-31, 2018, 10.1016/j.rse.2018.09.008.
[25] Kumar, V., and S. Agrawal, "Agricultural land use change analysis using remote sensing and GIS: a case study of Allahabad, India", International Archives of the Photogrammetry, Remote Sensing & Spatial Information Sciences, 2019, 10.5194/isprs-archives-XLII-3-W6-397-2019.

